Pharmaceutical Research, Vol. 26, No. 3, March 2009 (© 2008)
DOI: 10.1007/s11095-008-9786-x

Research Paper

Poly(Lactic-co-Glycolic) Acid as a Carrier for Imaging Contrast Agents

Amber L. Doiron,[1] Kimberly A. Homan,[1] Stanislav Emelianov,[1] and Lisa Brannon-Peppas[2,3]

Received September 9, 2008; accepted November 4, 2008; published online November 26, 2008

Purpose. With the broadening field of nanomedicine poised for future molecular level therapeutics, nano- and microparticles intended for the augmentation of either single- or multimodal imaging are created with PLGA as the chief constituent and carrier.
Methods. Emulsion techniques were used to encapsulate hydrophilic and hydrophobic imaging contrast agents in PLGA particles. The imaging contrast properties of these PLGA particles were further enhanced by reducing silver onto the PLGA surface, creating a silver cage around the polymeric core.
Results. The MRI contrast agent Gd-DTPA and the exogenous dye rhodamine 6G were both encapsulated in PLGA and shown to enhance MR and fluorescence contrast, respectively. The silver nanocage built around PLGA nanoparticles exhibited strong near infrared light absorbance properties, making it a suitable contrast agent for optical imaging strategies such as photoacoustic imaging.
Conclusions. The biodegradable polymer PLGA is an extremely versatile nano- and micro-carrier for several imaging contrast agents with the possibility of targeting diseased states at a molecular level.

KEY WORDS: fluorescence; Gd-DTPA; magnetic resonance imaging (MRI); photoacoustic ultrasound (PAUS) imaging; silver.

INTRODUCTION

The newly termed field of nanomedicine, as defined by the United States' National Institutes of Health Roadmap for Medical Research in Nanomedicine (1), aims to apply technology with nanoscale features or technology aimed at nanoscale pathophysiology in order to increase specificity of treatment on a molecular level and improve human health. As an adjunct to this therapeutic goal, the field of imaging is called upon to improve molecular and clinical imaging in the hope of identifying the pathophysiology itself, tracking the therapeutic vehicle, monitoring disease changes, and determining an appropriate end-state to therapy. In many cases, imaging is necessary in the diagnosis of a diseased state prior to initiating therapy. Many clinical imaging methods are augmented by the use of contrast agents during imaging to further highlight differences between tissues. Agents can be encapsulated in order to restrict delivery of the contrast agents to a small area with possible targeting capabilities. In the emerging field of molecular imaging, multimodality of a contrast agent leads to novel insights. In this work, we adapted typical drug delivery methods for imaging agents with the augmentation of the following modalities: fluorescence microscopy, magnetic resonance imaging (MRI), and photoacoustic ultrasound (PAUS) imaging.

Drug delivery to physiological sites of interest is a widely researched area due to the potential benefits of a reduction in systemic side effects, increased drug efficacy at the site of interest, and delivery of a potent dose directly to the diseased tissue. Drug delivery focuses on the use of a carrier and possibly the incorporation of active targeting through the use of a chemical or physical scheme to concentrate an active agent at a site of action with various other possible functionalities built into the system. One of the most widely investigated materials in drug delivery is poly(lactic-*co*-glycolic) acid (PLGA) due to its long history in the field, many advantageous properties, ease of use and wide availability (2,3).

Polylactic acid (PLA) and PLGA, the FDA-approved polymer of lactic acid and the copolymer of lactide and glycolide, are the principle structural components of the formulated particles intended for imaging detailed here. PLA and PLGA are biodegradable polymers that are approved for use as suture material and in various drug delivery systems, including Lupron Depot®, ProLease® and Trelstar® Depot (3,4). PLGA degrades into lactic acid and glycolic acid through hydrolysis of the ester bond, and the material bulk erodes as water diffuses into the matrix more quickly than the polymer degrades (5,6). PLGA is biocompatible due to the uptake of lactide and glycolide post-degradation into the citric acid cycle, and this allows for the use of PLGA without need for removal of the material after the intervention. PLGA particles have been formulated extensively for delivery using both oral and subcutaneously-injected delivery systems (7,8). Furthermore, biodegradable PLGA nanoparticles have been utilized as successful delivery systems (3,5,9–11).

[1] Department of Biomedical Engineering, The University of Texas at Austin, Austin, TX, USA.
[2] Appian Labs, Austin, TX, USA.
[3] To whom correspondence should be addressed. (e-mail: lpeppas@etibio.com)

Due to their size and shape, nanoparticles and microparticles are popular for the encapsulation and delivery of active agents due to their ability to travel through blood vessels or be injected into other physiological areas such as the peritoneum and protect the encapsulated agent until delivery. Particles offer several advantages over other delivery schemes including their high surface area that augments release properties and allows for attachment of targeting agents or other materials to the surface, the modification of the biodistribution of the active agent in a controlled manner, the ability to move within the bloodstream and target to a desired location through the use of a targeting scheme, and their ability to deliver to any vascularized physiological areas if injected intravenously and of appropriate size (12–14). Particles of PLGA can be formulated in many ways (3,13,15,16), yet we have demonstrated the utility of emulsion and nanoprecipitation techniques (17–20) for the encapsulation of both hydrophilic and hydrophobic agents. The advantages of the emulsion techniques are simplicity, flexibility in size by adjusting chemical interactions between starting materials, and the ability to encapsulate an agent without chemically linking it to the carrier. The optimization (18) and scale up production (19) of PLGA particles up to 100 g per batch have been reported by our research group.

Despite its widespread use in drug delivery schemes (3), PLGA has been studied much less frequently for applications involving imaging technology. When particles are used with imaging applications in mind, they are typically researched as an adjuvant to therapy by tracking particle paths or tracking the release of drug. Here we show the utility of PLGA particles for several imaging modalities including fluorescence microscopy, magnetic resonance imaging, and photoacoustic/ultrasound imaging.

Although fluorescence imaging is not used in clinical human applications, it is very important for *in vitro* studies as well as work in small animals. Many different molecules can be used for fluorescence including drug molecules so long as a fluorophore is present within the molecule (21,22). This demonstrates an increasing versatility of the particle scheme for both imaging and therapy (17). Particle tracking in both cell studies and animal studies is vital to the understanding of the efficacy of drug delivery (3,14,21–23). Rhodamine 6G is chosen here as a fluorescent molecule with excellent photostability and extensive previous characterization of properties.

MRI is a powerful, non-invasive clinical technique for anatomical imaging that is enhanced by the use of contrast agents and is useful in the detection of various diseases. MRI has excellent spatial resolution, is noninvasive, and is sequentially repeatable to track disease changes due to its lack of ionizing radiation. MRI can create several anatomical images based on biophysical and biochemical parameters with differing contrast by varying only imaging parameters, and several contrast agents exist that augment imaging with very low risk of adverse reaction. The quality of images derived from MRI and its safety has made it one of the fastest growing modalities. MRI can also be used to visualize the vasculature using special imaging sequences or a blood contrast agent which is important in many diseases such as atherosclerosis. The in-plane spatial resolution of MRI using a conventional 1.5 Tesla scanner is approximately 1 mm while the temporal resolution is on the order of seconds. The available signal, contrast, and lack of noise contribute to the ability to create high quality images (24). The limited specificity and low inherent sensitivity of MRI highlight the utility of a physiology-specific imaging agent to increase contrast in an area of interest. The positive MR contrast agent gadolinium diethylenetriaminepentaacetic acid (Gd-DTPA) and close derivatives are FDA-approved, have a long history in MRI, are hydrophilic, and have been encapsulated in small amounts previously for tracking of drug delivery, for neutron capture, and for MR imaging (21,25–30).

In comparison to MRI, combined photoacoustic and ultrasound imaging is a new technique that is gaining momentum (31–34). PAUS imaging takes advantage of the clinically-proven, low cost ultrasound modality and adds to it an optical component necessary for photoacoustic wave generation. Short, nanosecond pulses of laser light are shone on the imaging target. Any nanoparticle, contrast agent, or component of tissue that absorbs light strongly at the incident wavelength generates corresponding pressure, or "acoustic", waves in response to the pulsed incident light. These acoustic waves are captured by an ultrasound transducer and co-registered with an ultrasound image of the same area. If nanoparticles designed specifically to absorb light at the incident wavelength are located in diseased tissue, PAUS imaging shows enhanced contrast of the area. Therefore, the nanoparticles act as the contrast agents, and PAUS imaging provides the location of these nanoparticles against the general anatomical grey-scale images already captured by ultrasound. This technique is naturally limited by the resolution of conventional ultrasound and the penetration of light into tissue (light penetration is several centimeters using wavelengths between 700–1,000 nm). However, PAUS is considerably more robust than ultrasound alone, providing real-time contrast enhancement of myriad diseased states.

In this paper, we discuss the encapsulation or attachment of imaging contrast agents into or onto PLGA particles for the augmentation of imaging in a specific location as an initial step in nanomedicine where nano-features or nanoscale pathophysiology indicate the necessity for medical intervention. Several particle types are detailed here including PLGA particles of various size distributions entrapping the MR contrast agent Gd-DTPA and/or the fluorescent agent rhodamine 6G. Additionally, particles with or without rhodamine 6G entrapped in the PLGA and constructed with an exterior silver cage are described here for their use in photoacoustic imaging. The different PLGA particle types constructed are shown pictorially (Fig. 1).

MATERIALS AND METHODS

Materials

All chemicals were used without further purification. PLGA 50:50DL 2A was purchased from Lakeshore Biomaterials (Birmingham, AL, USA, inherent viscosity (~0.5% chloroform) 0.16 dL/g, 52.8:47.2 lactide to glycolide ratio) and Medisorb (Cincinnati, OH, M_n=11 kD, polydispersity 1.7, inherent viscosity 0.17 dL/g, 53:47 lactide to glycolide ratio). Rhodamine 6G, ACS grade L(+) ascorbic acid, lecithin, and

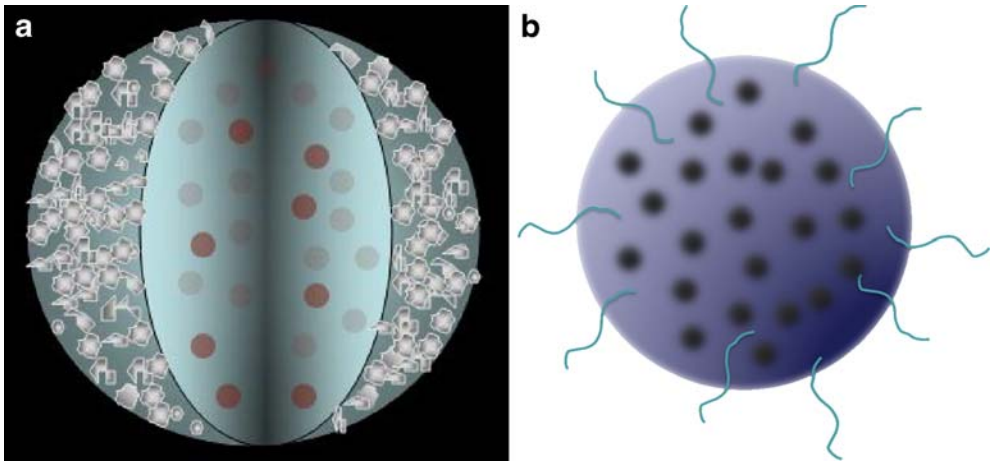

Fig. 1. **a** PLGA core with entrapped fluorescent contrast agents and a porous silver outer cage required to enhance optical imaging contrast. **b** PLGA matrix with entrapped MR or fluorescent contrast agents.

ultrapure silver nitrate were products of Acros (Morris Plains, NJ, USA). Hexane was purchased from Acros in Geel, Belgium. Polyvinyl alcohol (PVA), mineral oil, and diethylenetriaminepentaacetic acid gadolinium (III) dihydrogen salt hydrate (Gd-DTPA) were purchased from Sigma-Aldrich (St. Louis, MO, USA). Dimethyl sulfoxide (DMSO), agarose, and acetone were purchased from Fisher Scientific (Fair Lawn, NJ, USA). Slide mounting media, Vectashield, was from Vector Laboratories (Burlingame, CA, USA). Sodium hydroxide was purchased from J.T. Baker (Phillipsburg, NJ, USA). Human umbilical vein endothelial cells (HUVEC) and endothelial growth medium (EGM) were used from Lonza, formerly Clonetics (Walkersville, MD, USA). Gelatin was from Difco supplied by Beckton, Dickerson and Company (Sparks, MD, USA) and Dulbecco's phosphate buffered saline (DPBS) came from Mediatech, Inc. (Herndon, VA, USA). Poly(lactic acid)-poly(ethylene glycol) block copolymer was prepared by ring opening polymerization of *d*,*l*-lactide monomer (Polysciences, Inc., Warrington, PA) onto carboxymethyl-PEG-OH (MW 3400, Laysan Bio, Inc., Arab, AL) in the presence of stannous 2-ethylhexanoate (Sigma) in toluene (anhydrous, Acros), and the product was recovered after dissolution in methylene chloride (Fisher Scientific) and precipitation in ethyl ether (anhydrous, Fisher Scientific).

Methods

Particles for MR Imaging

As has been described previously (20), a water-in-oil-in-oil (W/O/O) double emulsion technique based on work by Chaw and colleagues (35) was employed to encapsulate the hydrophilic agent diethylenetriaminepentaacetic acid gadolinium (III) dihydrogen salt for use in MR imaging. Targeted loading levels of Gd-DTPA were in the range of 5 to 35 wt.%. Briefly, Gd-DTPA dissolved in deionized (34) water containing surfactant was added to an acetone solution containing PLGA and was sonicated at 45 W output power. This emulsion was then transferred into the external phase of mineral oil containing lecithin, and the double emulsion was sonicated at either 45 or 120 W output power to create two distinct size distributions. After solvent evaporation, particles were collected with centrifugation at 45,000×*g* for 15 min, washed twice with hexane, frozen, and freeze dried before use. As an alternative, poly(lactide)-*block*-poly(ethylene glycol) (PLA-PEG) of approximately 50 kD as prepared by ring opening polymerization as described previously (20,36) was used instead of PLGA using 45 W sonication for both emulsion steps in order to create a third Gd-DTPA-containing particle type without modification of the protocol.

Particles for Fluorescent Microscopy

In much the same way, rhodamine 6G was encapsulated in PLGA micro- and submicron-particles using the W/O/O method with the substitution of rhodamine in the aqueous phase for Gd-DTPA with targeted loading ranging from 0.05% to 0.6%. No additional modifications were made in the formulation process for encapsulation of this agent, and rhodamine was also encapsulated in the PLA-PEG polymer. Additionally, both Gd-DTPA and rhodamine 6G were encapsulated in the same particles by combining both agents at appropriate targeted loadings in the aqueous phase of the emulsion to create a multimodal particle.

Alternatively, PLGA nanoparticles were produced using an oil-in-water (O/W) nanoprecipitation method previously described (17). Briefly, 50 mg of PLGA were dissolved in 2 ml of acetone to create the oil phase. This oil phase was then added to 10 ml of a water phase consisting of 10 mg/ml polyvinyl alcohol in deionized water. The oil-in-water emulsion was sonicated at 45 W for 15 s, and the acetone was removed by stirring under vacuum for 20 min at room temperature. The milky-white suspension was then centrifuged at 45,000×*g* for 15 min to recover the PLGA nanoparticles and remove excess PVA. The supernatant was discarded and the PLGA nanoparticles were either used immediately or frozen and freeze dried for prolonged storage.

Particles for Photoacoustic and Ultrasound Imaging

PLGA-Ag nanocages were produced using a bottom–up approach. After creation of the PLGA particles by either W/O/O or O/W emulsion techniques, silver was photoreduced onto the PLGA core, requiring the presence of a primary

alcohol. Thus, the surfactant PVA that was already available on the surface of the PLGA nanoparticles created by O/W techniques was used. Alternatively, the W/O/O PLGA particles were soaked in a 10 mg/ml PVA solution in DI water for 20 min prior to photoreduction. Then, in a shallow, wide glass dish, 29.5 ml of DI water and 0.2 ml of 0.15 M silver nitrate solution were mixed with 0.5 ml of a 5 mg/ml PLGA particle suspension. An 8 W ultraviolet (UV) 254 nm light source irradiated the stirring sample for 20 min (thickness of the sample transverse to the light path was no greater that 3 mm to allow for maximum UV light exposure) in order to form tiny seeds of silver on the PLGA surface. The silver seeded PLGA nanoparticles were removed from the light, and under continued stirring, 100 μL of 18% ascorbic acid was added at room temperature. Silver reduction was complete after 2 min and the pH of the solution dropped to 4.5. To bring the pH back to 7 (to avoid accelerated PLGA degradation), 100 μL of 1 N sodium hydroxide was added. For storage, the particles were centrifuged at 45,000×*g* for 15 min, the supernatant was decanted, and particles were kept at −20°C.

Particle Characterization

Particles were characterized on the basis of morphology, encapsulation and loading, and the ability to augment image contrast. In order to examine morphology and qualitatively judge size, PLGA particles were suspended in DI water with sonication, a drop placed on carbon conductive tape on a scanning electron microscope (SEM) platform, and allowed to dry prior to sputter coating with gold. Imaging was performed on a Hitachi S-4500 field emission scanning electron microscope at 10 kV accelerating voltage. Silver coated particles did not require sputter coating prior to imaging and were imaged at a 10 kV accelerating voltage on a LEO 1530 scanning electron microscope. Additionally, W/O/O PLGA particles were examined on a Philips EM 208 transmission electron microscope (27) in order to accurately visualize the smaller particles in the distribution.

The surface charge and size distribution of PLGA particles produced using the O/W emulsion method were characterized using a ZetaPlus instrument with accompanying software (Brookhaven Instruments Corp., Holtsville, NY) on suspensions of 1 mg/mL particles in a 1 mM KCl electrolyte solution.

The encapsulation efficiency as well as loading of Gd-DTPA in the particles was determined as published previously (20) using inductively coupled plasma-mass spectrometry (ICP-MS). ICP-MS was also used to quantify the amount of silver reduced during the formation of the PLGA-Ag nanocages. PLGA-Ag particles were dissolved in a 70% nitric acid solution to prevent aggregation and disruption of sample flow through the ICP nozzle.

The encapsulation efficiency of rhodamine 6G was determined by first dissolving the particles in DMSO and then determining the absorbance at a wavelength of 536 nm using an ultraviolet/visible spectrophotometer (Shimadzu UV-1201, Japan) along with standards of various concentrations of rhodamine 6G dissolved in DMSO. The same spectrophotometer was also used to obtain the extinction spectrum of the PLGA-Ag nanocages. Directly following the ascorbic acid induced reduction of the PLGA-Ag nanocages, 2.0 ml of the suspension was placed in a cuvette of path length 10 mm. An extinction spectrum from the visible to near infrared wavelengths was captured for the PLGA-Ag nanocages.

Confocal Imaging of Rhodamine Particles

Rhodamine-containing particles were utilized for particle-tracking *in vitro* with human umbilical vein endothelial cells (HUVEC) and were imaged using a confocal laser scanning microscope. Pooled HUVEC at passage 3 were cultured for 48 h in endothelial growth medium (EGM) at 37° C with 5% CO_2 in a six-well plate containing six pre-sterilized glass coverslips coated with 1% gelatin in Dulbecco's PBS (DPBS) for 1 h prior to cell plating. Cells were exposed to rhodamine 6G-loaded W/O/O PLGA particles (targeted loading 0.1 wt.%, 120 W sonication), PLA-PEG particles containing rhodamine (targeted loading 0.5 wt.%, 45W sonication), PLGA particles containing no active agent, and PLA-PEG particles containing no active agent suspended in media at both 10 and 1 μg/mL, as well as media only for 1 h. Cells were washed three times with cold DPBS and incubated with 4% formaldehyde for 20 min for fixation. Coverslips

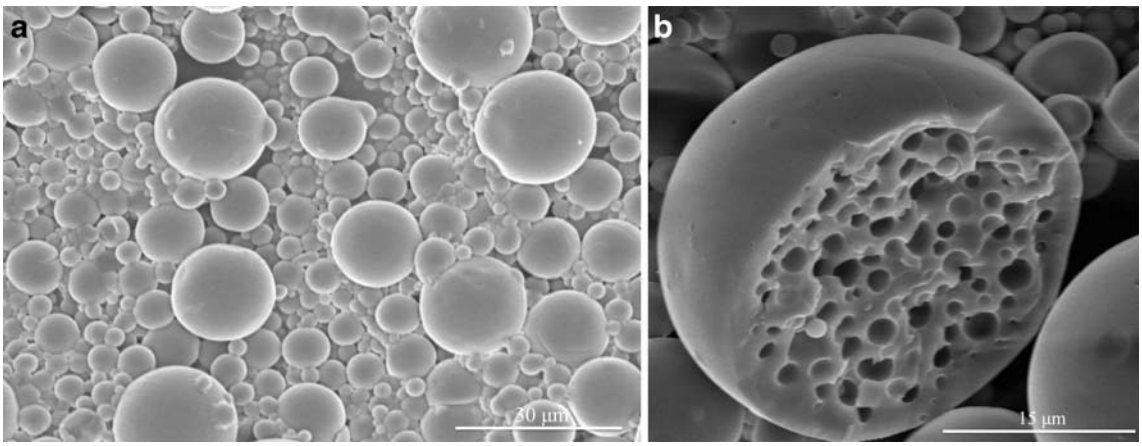

Fig. 2. **a** SEM image of PLGA W/O/O microparticles formed using 45 W sonication for both emulsions. **b** SEM image of one split microparticle showing the interior morphology of the formed polymeric particle.

were removed from formaldehyde solution, lightly blotted to remove excess liquid, and secured to a clean glass slide using Vectashield containing the fluorescent agent DAPI for nuclear staining. Clear nail polish was used to seal the edges of the coverslip to the glass slide for long term storage at 4°C. Imaging of fixed cell samples exposed to fluorescent particles and appropriate controls was carried out on a Leica SP2 AOBS confocal microscope.

Magnetic Resonance Imaging of Particles

MRI studies of particles containing Gd-DTPA at various loadings were performed as described previously (20). Briefly, Gd-DTPA-containing PLGA and PLA-PEG particles as well as particles containing no active agents and samples with unencapsulated Gd-DTPA were suspended in agarose gel (1.5 wt.% prepared with deionized water) at concentrations of 0.5, 1, and 2 mg/mL until imaging in order to prevent settling and to slow release. *In vitro* r_1 and r_2 relaxivities were determined using a GE 1.5 T scanner (Excite, HD, GE Healthcare Technologies, Waukesha, WI) accompanied by a GE Quad Ankle coil using a 2D inversion recovery sequence for T_1 measurements and a 2D spin echo sequence for T_2 measurements. For T_1, the inversion recovery (2D IR) sequence used the following imaging parameters: TR=3,000 ms; TE=14 ms; TI=50, 70, 100, 200, 250, 300, 400, 500, 600, 700, 800, 900, 1,000, 2,000, 2,950 ms; a band width of 15.6 kHz; FOV of 18×9 cm; slice thickness of 4.0 mm; matrix of 256×128; and a flip angle of 90°. For T_2, the 2D SE sequence used TR=4,000 ms; TE=16, 20, 30, 40, 60, 80, 100, 200, 300 ms; band width of 15.6 kHz; FOV of 18×9 cm; slice thickness of 4.0 mm; matrix of 256×128; and flip angle of 90°. Values for r_1 and r_2 were determined where r_1 and r_2 are the inverse of T_1 and T_2, respectively.

RESULTS

Electron microscopy techniques were used to visualize all particles. The morphology of the microparticles and submicron particles created by W/O/O double emulsion is shown clearly in the resulting scanning and transmission electron micrographs. Fig. 2a. shows the smooth surfaced, near-spherical, non-aggregated microparticles formed using 45 W sonication of average size around 5 μm. Rarely, a split or broken particle was seen within the samples, as shown in Fig. 2b., and the interior structure of the W/O/O particles was seen. W/O/O particles formed using 120 W sonication in the formation of the double emulsion were of smaller size, nearer to 1 μm and sub-micron in size (Fig. 3). TEM was used to visualize small particles including those of a truly nanoparticle size range (1–100 nm) formed using either sonication speed with the W/O/O method (Fig. 4). The encapsulation of either Gd-DTPA, rhodamine 6G, or the combination of the two agents did not affect the morphology as seen using these techniques.

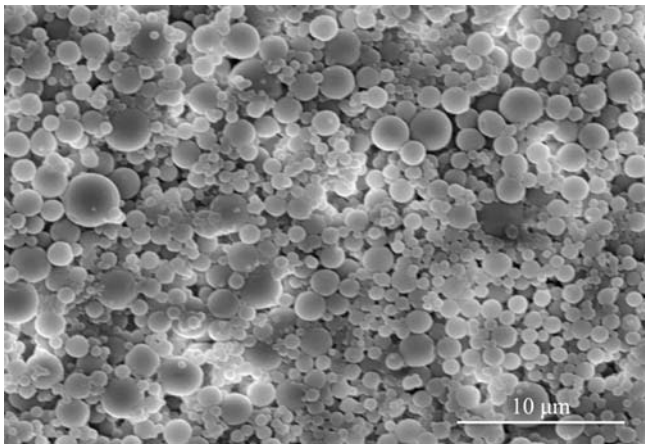

Fig. 3. SEM image of PLGA W/O/O submicron particles formed using 120 W sonication for the creation of the second emulsion.

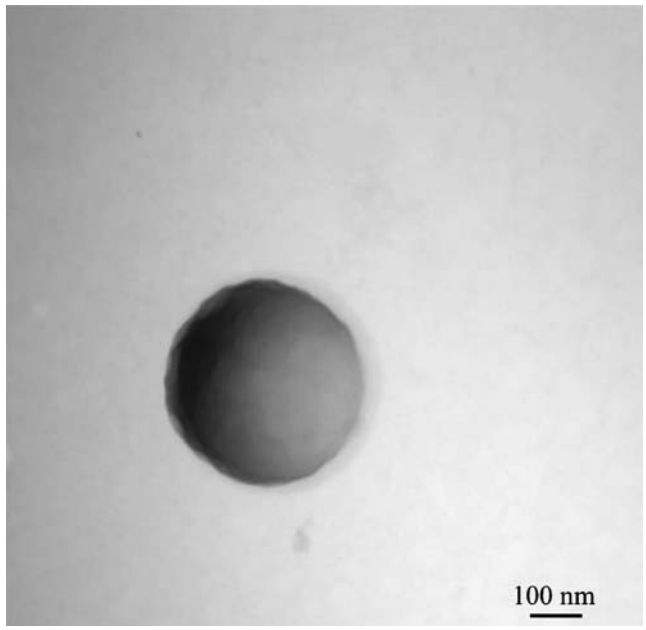

Fig. 4. Negatively stained image of small PLGA particle formed during W/O/O method using 45 W sonication for both emulsions.

Scanning electron micrographs of silver reduced onto the PLGA O/W particles are shown in Fig. 5. Specifically, the silver seeds produced during photoreduction on the PLGA surface are shown (Fig. 5a). Immediately upon addition of ascorbic acid to further reduce silver onto the seeds, the solution turned from a cloudy tan color to grey-black, finally settling to greenish-brown over the course of 2 min. The silver seeds growing on the PLGA surface were visualized at an intermediate step (Fig. 5b), before being reduced to silver cages (Fig. 5c). Additionally, particles encapsulating rhodamine (targeted loading 0.5%) were created with the W/O/O technique with 120 W sonication, and silver was subsequently reduced onto the PLGA surface. The resultant particles are shown in Fig. 6, and no effect of the encapsulant or different emulsion method is seen to affect the end product in morphology.

Sizes and zeta potentials of the W/O/O PLGA particles have been reported previously and are not reported here (20). The ability of the W/O/O technique to efficiently encapsulate hydrophilic Gd-DTPA has been published previously (20). The encapsulation efficiency achieved of rhodamine in PLGA particles formed with 120 W sonication averaged 40% with a typical range of 15% to 60%. Additionally, the encapsulation efficiency of rhodamine within PLA-PEG particles was typically between 10% and

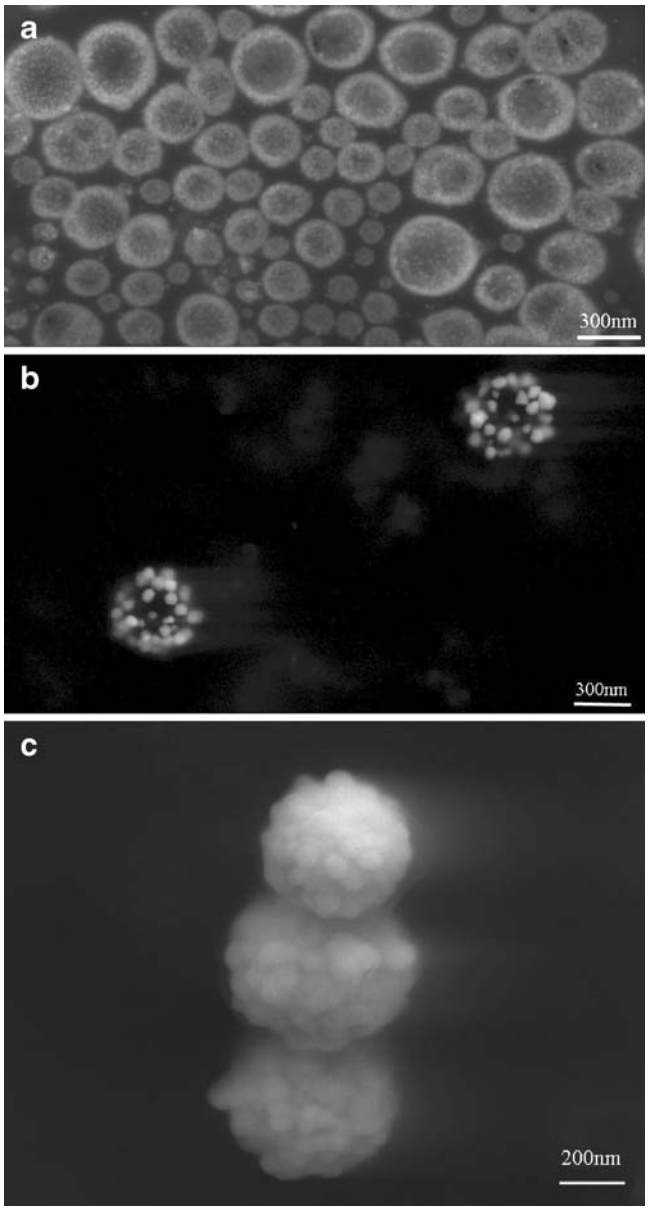

Fig. 5. PLGA-Ag nanocages at various stages of silver reduction, **a** silver seeds coating PLGA following photoreduction, **b** intermediate step in the ascorbic acid reduction where larger seeds on PLGA are present, **c** final porous cage configuration of silver on PLGA at the completion of ascorbic acid silver reduction.

30%. Loading of rhodamine within the submicron particles was near 0.1%, being more than sufficient to fluoresce under appropriate excitation.

HUVEC under normal culture conditions were exposed to particles encapsulating rhodamine of various sizes in order to determine the location of the particles after 1 h. As seen in Fig. 7, the rhodamine particles are easily seen using confocal microscopy with appropriate excitation and emission wavelengths. Fig. 7 shows the overlay of an image of the fluorescing rhodamine PLA-PEG particle located near the cell surface as seen with transmitted light, and the nucleus is fluorescently stained blue with DAPI. Although not fully elucidated by this image, both PLGA and PLA-PEG particles of roughly 100 nm to 1 μm containing rhodamine were observed within the endothelial cells after this 1 h time point.

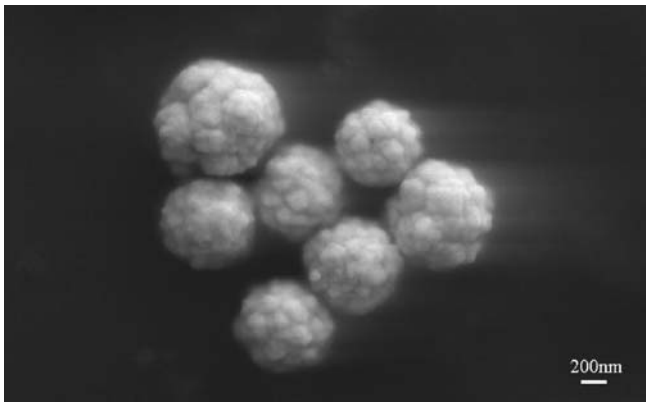

Fig. 6. SEM image of the W/O/O particles with encapsulated rhodamine and a silver cage on the exterior of the particle.

Particles containing no fluorescent agent were slightly visible under transmitted light microscopy; however, it was difficult to differentiate these particles from debris, and the smaller particles were not visible at all.

PLGA particles created by O/W nanoprecipitation averaged 220 nm in mean diameter with a polydispersity index of 0.11 and a zeta potential of −9 mV as measured using a ZetaPlus instrument. ICP-MS confirmed that 95% of the silver used to produce the nanocages was incorporated into the silver cage and could be detected. The thickness of the porous silver layer around the PLGA core averaged 40–80 nm according to SEM analysis. The extinction spectrum of PLGA-Ag nanocages exhibited broad strong absorbance across the near infrared wavelengths (Fig. 8).

MRI scans of suspended particles were performed in order to determine the characteristic properties of Gd-DTPA-containing particles suspended in agarose gel. Results are

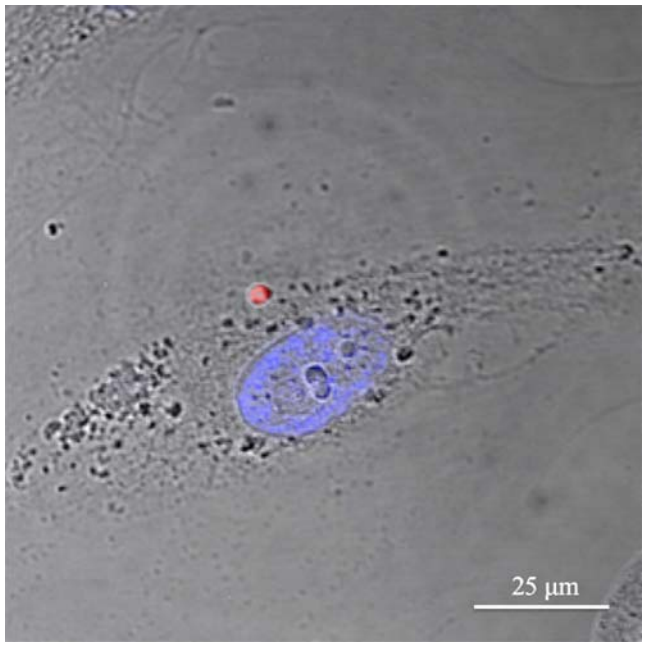

Fig. 7. Confocal microscopy image of rhodamine encapsulated in PLA-PEG W/O/O particle after exposure to HUVEC for 1 h. HUVEC nucleus stained with DAPI, and both fluorescence images overlaid on a light microscopy image all taken with a ×63 objective.

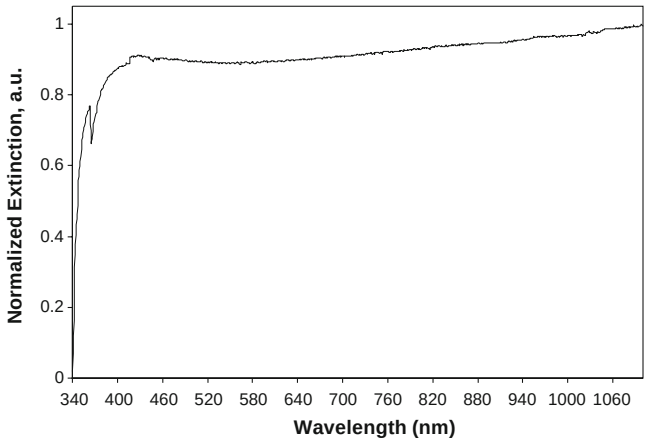

Fig. 8. Extinction spectrum of PLGA-Ag nanocages.

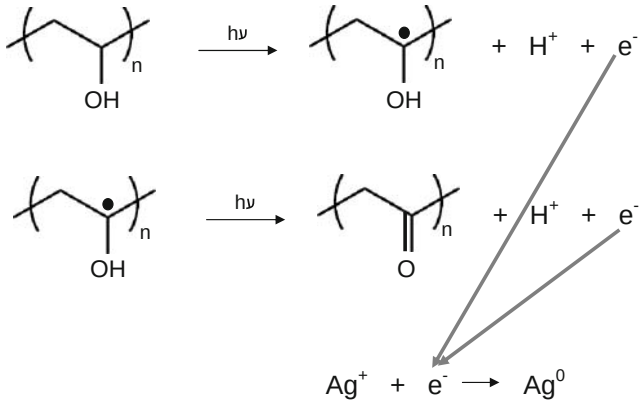

Fig. 10. Photoinduced oxidation of PVA leading to reduction of silver ions in solution.

shown in Fig. 9 expressed in r_1 compared to the concentration of particles at various loadings of Gd-DTPA. Both PLGA and PLA-PEG particles show a linear relationship between r_1 and concentration of particles. Additionally, agarose gels containing more than one particle type showed properties of the separate Gd-DTPA loadings and were distinguishable with the scan sequences performed (not shown). Particles affected contrast on images depending on the loading of the particles as well as the concentration of particles in the sample. Data collected concerning the relationship between r_2 and particle concentration are not shown because r_2 values did not statistically differ at the tested concentrations of particles or Gd-DTPA, as expected. Particles with no Gd-DTPA did not affect contrast, and PLA-PEG particles at similar loading to PLGA particles had similar MR responses in properties.

DISCUSSION

PLGA has been used for decades as a versatile biomaterial and has been researched extensively for drug delivery applications. PEG is included in some of these studies to demonstrate the possibility of the addition of 'stealth' properties onto these imaging particles as would likely be required for *in vivo* use (37). Here we have shown the utility of the polymer as a carrier for imaging agents for fluorescence, magnetic resonance imaging, and combined photoacoustic and ultrasound imaging. The use of PLGA for encapsulating both hydrophobic and hydrophilic agents has been demonstrated as well as the possibility of reducing silver on the surface of the PLGA particles. To the knowledge of these researchers, this is the first time the silver-PLGA particle conjugate has been demonstrated. Theoretically, the adaptability of this particle formulation is not limited by size requirements, imaging modality, biocompatibility, nor favorability of interactions with water.

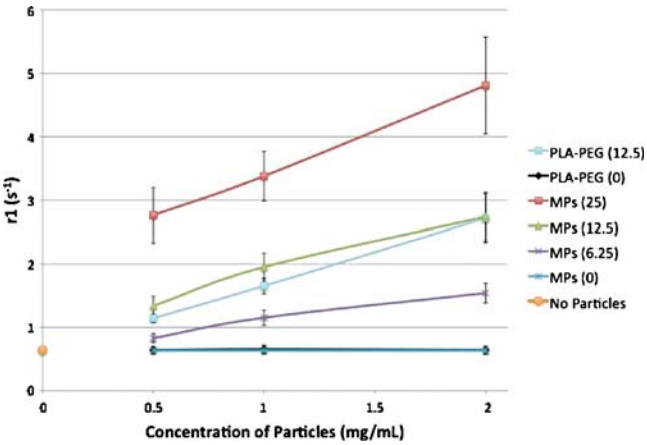

Fig. 9. Plot of r_1 values of particle formulations at different particle concentrations suspended in agarose gel for MR imaging. All particles formed using 45 W sonication. *Legend* indicates type of polymer used for encapsulation as well as targeted loading value in percent weight Gd-DTPA. Condition with no particles contained agarose gel only, while 0% loading conditions contain particles without active agent in agarose gel.

Although demonstrated before, the use of PLGA to encapsulate more than one imaging agent for utility in multimodal imaging as shown here is important for the future of nanomedicine. The ability to image the same particles with more than one imaging technique such as fluorescence microscopy allows researchers to follow the particles *in vitro* at a cellular level while also tracking the particles *in vivo* using a modality more appropriate for studies on an organism level such as MRI or PAUS. With future applications in mind, it is also possible to add molecular recognition capabilities to these anatomic imaging modalities by adding molecular targeting capabilities to the particle schemes. Multimodal imaging elucidates the mechanism of congregation at a site of action by enabling molecular and cellular study with the resolution of fluorescence imaging and correlation to clinical imaging techniques.

All PLGA and PLA-PEG particles were stable in solution as confirmed by the appearance of the Tyndall effect and confirmed quantitatively by zeta potential measurements. The PLGA particles made using PVA as a surfactant in the O/W method had a zeta potential of −9 mV, which is close to the range previously reported (17). Similarly, the W/O/O particles were stabilized by even higher repulsive forces, likely due to the presence of the emulsifier lecithin at the particle surface (20).

Sizes of the different particle types varied with the emulsion method employed. For instance, the O/W technique formed small PLGA particles in the range of 220 nm with low polydispersity, the W/O/O method with 120 W sonication formed submicron particles, and the W/O/O 45 W sonication method formed particles in the 1–30 μm range with some

particles below 100 nm as seen using TEM. Therefore, the utility of PLGA for imaging is broad as size can be tuned for application, whether it be intratumoral, intravascular, intraperitoneal, or another pathophysiological location.

To this end, PLGA and PLA-PEG particles containing rhodamine 6G were used for particle tracking *in vitro* with endothelial cells. Particles of sizes near 100 nm up to several microns were easily visible under fluorescence when excited with an appropriate wavelength of light. DAPI was used as a nuclear fluorescent stain in order to better visualize the cell structure. Very low loading of rhodamine was necessary in the particles due to the high quantum yield and photostability of rhodamine. These particle types release rhodamine very slowly *in vitro* in PBS at 37°C with less than 10% of the agent releasing within one month (results not shown). This adds to the utility of these particles for *in vitro* studies by allowing tracking of particles only instead of released dye. The high resolution of this optical technique aids researchers in particle tracking, and understanding the cellular biodistribution is important for establishment of safety and efficacy of delivery mechanisms.

The encapsulation of Gd-DTPA at high loadings has been previously reported by our group (20), and we show here the MR properties of the particles hold over a concentration range of 0.5 to 2 mg/mL, suggesting the possibility of quantification of particulate contrast agent at a given site of interest. This type of imaging involving a quantifiable agent combined with a molecular or cellular targeting scheme allows for the quantification of a given target in a pathophysiological site such as a tumor or atherosclerotic lesion. Combining the Gd-DTPA and rhodamine in a particle permits visualization of both the cellular mechanisms of targeting as well as the physiological results of a targeted contrast agent.

The construction of a silver cage around these particles allows for their tracking via other optical methods such as PAUS. The two step method used to build a silver cage over a PLGA particle allowed for reduction of silver directly onto the PLGA surface. Using photoreduction followed by ascorbic acid reduction, the reduced silver ions were associated with PLGA particles and minimal unattached silver colloid was found in solution. The use of PVA in photoreduction provided the spatial specificity for building silver seeds directly on the PLGA surface. PVA acted as both a reducing agent and macroscopic support for the growing silver seeds on the PLGA particle. The mechanism of photoreduction using PVA was similar to that reported elsewhere for gold reduction (38) (Fig. 10). In the second step, addition of ascorbic acid acted to further reduce silver onto the seeds started by photoreduction, maintaining silver growth specifically onto PLGA. Similar to PVA, the oxidation of ascorbic acid forms aldehyde groups from hydroxyl groups, yielding the final oxidized form of vitamin C, dehydroascorbic acid. Also, once ascorbic acid was added, Ostwald ripening was evident (Fig. 5b) where smaller silver seeds were amassed and pulled into larger growing seeds. Eventually these larger silver seeds touch and form the final porous silver nanocage around PLGA (Fig. 5c).

Due to the polydispersity in size and the layer of silver coating, silver nanocages exhibited a very broad extinction spectrum across the visible to NIR wavelengths (Fig. 8). In the NIR the extinction is high due mainly to light absorption. This NIR absorption will allow for these nanocages to act as contrast agents in photoacoustic imaging or various other optical imaging strategies.

The silver coated PLGA particles were termed nanocages *versus* nanoshells or nanospheres due to their porous nature. Nanocages were inherently built in a rough, porous manner to allow for diffusion of small encapsulated agents from inside the PLGA core to the external environment of the nanocage in future applications. As demonstrated here, PLGA particles encapsulating rhodamine using the W/O/O double emulsion method were coated with a silver cage, making a multifunctional imaging particle. Furthermore, future applications could include encapsulation of small molecule drugs in PLGA with an external silver nanocage. These drugs could diffuse through the cage and exhibit therapeutic effects while the particle is imaged through a combination of optical or photoacoustic imaging techniques.

The use of silver in biomedical applications has been controversial as some *in vitro* studies have shown silver to exhibit cytotoxic effects. Despite these findings, silver continues to be used in multiple applications such as silver coated catheters, orthopedic implants, and many medical devices (39–41). Silver's antibacterial properties have been well understood for centuries (42,43), which explains the extensive use of silver in the healing of burns (44). Other studies have shown silver to be non-cytotoxic (45), but it is recommended that silver cytotoxicity be further explored for the cell lines directly affected once these silver nanocages are employed for a specific, targeted application.

CONCLUSION

The biodegradable polymer PLGA and copolymer PLA-PEG were shown here to be suitable carriers of various imaging contrast materials, from exogenous dyes to metals. The emulsion techniques outlined to entrap both hydrophilic and hydrophobic contrast agents in PLGA and PLA-PEG can be expanded to other molecules of interest, making PLGA a highly versatile, biocompatible medium for myriad imaging or drug delivery applications.

ACKNOWLEDGEMENTS

Generous grants from the American Heart Association and the National Science Foundation Integrative Graduate Education and Research Traineeship Program (IGERT) funded this work.

REFERENCES

1. NIH, National Institute of Health Roadmap for Medical Research: Nanomedicine, 2006.
2. L. Brannon-Peppas. Polymers in controlled drug delivery. *Med. Plast. Biomater.* **4**:34–44 (1997).
3. R. C. Mundargi, V. R. Babu, V. Rangaswamy, P. Patel, and T. M. Aminabhavi. Nano/micro technologies for delivering macromolecular therapeutics using poly(D,L-lactide-*co*-glycolide) and its derivatives. *J. Control Release*. **125**:193–209 (2008). doi:10.1016/j.jconrel.2007.09.013.
4. M. S. Shive, and J. M. Anderson. Biodegradation and biocompatibility of PLA and PLGA microspheres. *Adv. Drug Deliv. Rev.* **28**:5–24 (1997). doi:10.1016/S0169-409X(97)00048-3.

5. L. Brannon-Peppas. Recent advances on the use of biodegradable microparticles and nanoparticles in controlled drug delivery. *Int. J. Pharm.* **116**:1–9 (1995). doi:10.1016/0378-5173(94)00324-X.
6. M. ChasinR. S. Langer. *Biodegradable polymers as drug delivery systems*, Marcel Dekker, New York, 1990.
7. D. Blanco, and M. J. Alonso. Protein encapsulation and release from poly(lactide-*co*-glycolide) microspheres: effect of the protein and polymer properties and of the co-encapsulation of surfactants. *Eur. J. Pharm. Biopharm.* **45**:285–294 (1998). doi:10.1016/S0939-6411(98)00011-3.
8. M. Vert, S. Li, and H. Garreau. Recent advances in the field of lactic acid/glycolic acid polymer-based therapeutic systems. *Macromol. Symp.* **98**:633–633 (1995).
9. S. S. Feng, L. Mu, K. Y. Win, and G. Huang. Nanoparticles of biodegradable polymers for clinical administration of paclitaxel. *Curr. Med. Chem.* **11**:413–424 (2004). doi:10.2174/0929867043455909.
10. R. A. Jain. The manufacturing techniques of various drug loaded biodegradable poly(lactide-*co*-glycolide) (PLGA) devices. *Biomaterials*. **21**:2475–2490 (2000). doi:10.1016/S0142-9612(00)00115-0.
11. J. Panyam, and V. Labhasetwar. Biodegradable nanoparticles for drug and gene delivery to cells and tissue. *Adv. Drug Deliv. Rev.* **55**:329–347 (2003). doi:10.1016/S0169-409X(02)00228-4.
12. M. Gaumet, A. Vargas, R. Gurny, and F. Delie. Nanoparticles for drug delivery: the need for precision in reporting particle size parameters. *Eur. J. Pharm. Biopharm.* **69**:1–9 (2008). doi:10.1016/j.ejpb.2007.08.001.
13. V. Lassalle, and M. L. Ferreira. PLA nano- and microparticles for drug delivery: an overview of the methods of preparation. *Macromol. Biosci.* **7**:767–783 (2007). doi:10.1002/mabi. 200700022.
14. Y. Liu, H. Miyoshi, and M. Nakamura. Nanomedicine for drug delivery and imaging: a promising avenue for cancer therapy and diagnosis using targeted functional nanoparticles. *Int. J. Cancer.* **120**:2527–2537 (2007). doi:10.1002/ijc.22709.
15. G. A. Silva, P. Ducheyne, and R. L. Reis. Materials in particulate form for tissue engineering. 1. Basic concepts. *J. Tissue Eng. Regen. Med.* **1**:4–24 (2007). doi:10.1002/term.2.
16. C. E. Astete, and C. M. Sabliov. Synthesis and characterization of PLGA nanoparticles. *J. Biomater. Sci. Polym. Ed.* **17**:247–289 (2006). doi:10.1163/156856206775997322.
17. T. Betancourt, B. Brown, and L. Brannon-Peppas. Doxorubicin-loaded PLGA nanoparticles by nanoprecipitation: preparation, characterization and *in vitro* evaluation. *Nanomed.* **2**:219–232 (2007). doi:10.2217/17435889.2.2.219.
18. D. T. Birnbaum, J. D. Kosmala, and L. Brannon-Peppas. Optimization of preparation techniques for poly(lactic acid-*co*-glycolic acid) nanoparticles. *J. Nanopart. Res.* **2**:173–181 (2000). doi:10.1023/A:1010038908767.
19. L. Brannon-Peppas, and D. T. Birnbaum. Process to scale-up the production of biodegradable nanoparticles. Abstract, American Institute of Chemical Engineers Meeting. (2000).
20. A. L. Doiron, K. Chu, A. Ali, and L. Brannon-Peppas. Preparation and initial characterization of biodegradable particles containing gadolinium-DTPA contrast agent for enhanced MRI. Proceedings of the National Academy of Sciences. (in press).
21. W. J. Mulder, G. J. Strijkers, J. W. Habets, E. J. Bleeker, D. W. van der Schaft, G. Storm, G. A. Koning, A. W. Griffioen, and K. Nicolay. MR molecular imaging and fluorescence microscopy for identification of activated tumor endothelium using a bimodal lipidic nanoparticle. *Faseb J.* **19**:2008–2010 (2005).
22. A. Tsourkas, V. R. Shinde-Patil, K. A. Kelly, P. Patel, A. Wolley, J. R. Allport, and R. Weissleder. *In vivo* imaging of activated endothelium using an anti-VCAM-1 magnetooptical probe. *Bioconjug. Chem.* **16**:576–581 (2005). doi:10.1021/bc050002e.
23. T. Betancourt, K. Shah, and L. Brannon-Peppas. Rhodamine-loaded poly(lactic-co glycolic acid) nanoparticles for investigation of *in vitro* interactions with breast cancer cells. J Mater Sci: Mater Med. (online publication Sept. 25, 2008, print copy in press).
24. Z. A. Fayad, and V. Fuster. Clinical imaging of the high-risk or vulnerable atherosclerotic plaque. *Circ. Res.* **89**:305–316 (2001). doi:10.1161/hh1601.095596.
25. A. L. Ayyagari, X. Zhang, K. B. Ghaghada, A. Annapragada, X. Hu, and R. V. Bellamkonda. Long-circulating liposomal contrast agents for magnetic resonance imaging. *Magn. Reson. Med.* **55**:1023–1029 (2006). doi:10.1002/mrm.20846.
26. A. Z. Faranesh, M. T. Nastley, C. Perez de la Cruz, M. F. Haller, P. Laquerriere, K. W. Leong, and E. R. McVeigh. *In vitro* release of vascular endothelial growth factor from gadolinium-doped biodegradable microspheres. *Magn. Reson. Med.* **51**:1265–1271 (2004). doi:10.1002/mrm.20092.
27. B. Gimi, A. P. Pathak, E. Ackerstaff, K. Glunde, D. Artemov, and Z. M. Bhujwalla. Molecular Imaging of Cancer: Applications of Magnetic Resonance Methods. *Proc. IEEE*. **93**:784–799 (2005). doi:10.1109/JPROC.2005.844266.
28. T. N. Parac-Vogt, K. Kimpe, S. Laurent, C. Pierart, L. V. Elst, R. N. Muller, and K. Binnemans. Gadolinium DTPA-monoamide complexes incorporated into mixed micelles as possible MRI contrast agents. *Eur. J. Inorg. Chem.* **35**:38–43 (2004). doi:10.1002/ejic.200400187.
29. K. F. Pirollo, J. Dagata, P. Wang, M. Freedman, A. Vladar, S. Fricke, L. Ileva, Q. Zhou, and E. H. Chang. A tumor-targeted nanodelivery system to improve early MRI detection of cancer. *Mol. Imaging*. **5**:41–52 (2006).
30. H. Tokumitsu, H. Ichikawa, and Y. Fukumori. Chitosan-gadopentetic acid complex nanoparticles for gadolinium neutron-capture therapy of cancer: preparation by novel emulsion-droplet coalescence technique and characterization. *Pharm. Res.* **16**:1830–1835 (1999). doi:10.1023/A:1018995124527.
31. R. A. Kruger, P. Liu, Y. R. Fang, and C. R. Appledorn. Photoacoustic ultrasound (PAUS)-reconstruction tomography. *Med. Phys.* **22**:1605–1609 (1995). doi:10.1118/1.597429.
32. M. Xu, and L. V. Wang. Photoacoustic imaging in biomedicine. *Rev. Sci. Instrum.* **77**:041101 (2006). doi:10.1063/1.2195024.
33. J. J. Niederhauser, M. Jaeger, R. Lemor, P. Weber, and M. Frenz. Combined ultrasound and optoacoustic system for real-time high-contrast vascular imaging *in vivo*. *IEEE. Trans. Med. Imaging*. **24**:436–440 (2005). doi:10.1109/TMI.2004.843199.
34. S. Park, J. Shah, S. R. Aglyamov, A.B. Karpiouk, S. Mallidi, A. Gopal, H. Moon, X. J. Zhang, W. G. Scott, and S. Y. Emelianov. Integrated system for ultrasonic, photoacoustic and elasticity imaging. Medical Imaging 2006: ultrasonic imaging and signal processing. Edited by Emelianov, Stanislav; Walker, William F. *Proc. SPIE*. **6147**:148–155 (2006).
35. C. S. Chaw, Y. Y. Yang, I. J. Lim, and T. T. Phan. Water-soluble betamethasone-loaded poly(lactide-*co*-glycolide) hollow microparticles as a sustained release dosage form. *J. Microencapsul.* **20**:349–359 (2003). doi:10.1080/0265204021000058447.
36. P. Quellec, R. Gref, L. Perrin, E. Dellacherie, F. Sommer, J. M. Verbavatz, and M. J. Alonso. Protein encapsulation within polyethylene glycol-coated nanospheres. I. Physicochemical characterization. *J. Biomed. Mater. Res.* **42**:45–54 (1998). doi:10.1002/(SICI)1097-4636(199810)42:1<45::AID-JBM7>3.0.CO;2-O.
37. D. E. Owens 3rd, and N. A. Peppas. Opsonization, biodistribution, and pharmacokinetics of polymeric nanoparticles. *Int. J. Pharm.* **307**:93–102 (2006). doi:10.1016/j.ijpharm.2005.10.010.
38. A. Pucci, M. Bernabo, P. Elvati, L. I. Meza, F. Galembeck, C. A. dP. Leite, N. Tirelli, and G. Ruggeri. Photoinduced formation of gold nanoparticles into vinyl alcohol based polymers. *J. Mater. Chem.* **16**:1058–1066 (2006). doi:10.1039/b511198f.
39. C. A. Collinge, G. Goll, D. Seligson, and K. J. Easley. Pin tract infections: silver *vs* uncoated pins. *Orthopedics*. **17**:445–448 (1994).
40. G. Gosheger, J. Hardes, H. Ahrens, A. Streitburger, H. Buerger, M. Erren, A. Gunsel, F. H. Kemper, W. Winkelmann, and C. Von Eiff. Silver-coated megaendoprostheses in a rabbit model—an analysis of the infection rate and toxicological side effects. *Biomaterials*. **25**:5547–5556 (2004). doi:10.1016/j.biomaterials. 2004.01.008.
41. J. M. Schierholz, L. J. Lucas, A. Rump, and G. Pulverer. Efficacy of silver-coated medical devices. *J. Hosp. Infect.* **40**:257–262 (1998). doi:10.1016/S0195-6701(98)90301-2.
42. Hippocrates, On Ulcers. 400 B.C.E.; Translated by Francis Adams, ©, 1994–2000.
43. J. L. Clement, and P. S. Jarrett. Antibacterial silver. *Met.-Based Drug.* **1**:467–482 (1994). doi:10.1155/MBD.1994.467.
44. B. S. Atiyeh, M. Costagliola, S. N. Hayek, and S. A. Dibo. Effect of silver on burn wound infection control and healing: Review of the literature. Burns. (2006).
45. D. W. Brett. A discussion of silver as an antimicrobial agent: alleviating the confusion. *Ostomy Wound Manage*. **52**:34–41 (2006).